BNL-229186-2025-JAAM

GRP-ACM-159

Giant Cloud Condensation Nuclei Facilitate Drizzle Formation in Stratocumulus-Insights From a Combined ObservationModeling Framework

Z. Zhu

To be published in "Journal of Geophysical Research: Atmospheres"

November 2025

Environmental Science and Technologies Department

Brookhaven National Laboratory

U.S. Department of Energy

USDOE Office of Science (SC), Biological and Environmental Research (BER)

DISCLAIMER

Giant Cloud Condensation Nuclei Facilitate Drizzle Formation in Stratocumulus—Insights From a Combined Observation-Modeling Framework

Zeen Zhu[1], Fan Yang[1], Maria Zawadowicz[1], Alfonso Ladino Rincon[2], Jenna Ritvanen[3], Samantha Lankowicz[4], Kaylee H. Lundstrom[2], and Taylor Fitzgerald[4]

[1]Environmental Science and Technologies Department, Brookhaven National Laboratory, Upton, NY, USA, [2]Department of Climate, Meteorology and Atmospheric Sciences, University of Illinois at Urbana Champaign, Urbana, IL, USA, [3]Finnish Meteorological Institute, Helsinki, Finland, [4]School of Marine and Atmospheric Sciences, Stony Brook University, Stony Brook, NY, USA

- A novel framework integrates in situ, remote sensing, and an idealized model to study the effect of Giant Cloud Condensation Nuclei (GCCN) in drizzle initiation
- GCCN accelerates drizzle formation through condensation and enhanced collision-coalescence processes
- Model-observation consistency supports the effect of GCCN on drizzle formation

Correspondence to:

Z. Zhu,
zzhu1@bnl.gov

Citation:

Zhu, Z., Yang, F., Zawadowicz, M., Ladino Rincon, A., Ritvanen, J., Lankowicz, S., et al. (2025). Giant cloud condensation nuclei facilitate drizzle formation in stratocumulus—Insights from a combined observation-modeling framework.

Received 30 JUN 2025
Accepted 3 NOV 2025

Author Contributions:

Conceptualization: Zeen Zhu
Investigation: Zeen Zhu, Fan Yang
Methodology: Zeen Zhu, Fan Yang
Validation: Zeen Zhu, Fan Yang, Maria Zawadowicz, Alfonso Ladino Rincon, Jenna Ritvanen, Samantha Lankowicz, Kaylee H. Lundstrom, Taylor Fitzgerald
Writing – original draft: Zeen Zhu
Writing – review & editing: Zeen Zhu, Fan Yang, Maria Zawadowicz, Alfonso Ladino Rincon, Jenna Ritvanen, Samantha Lankowicz, Kaylee H. Lundstrom, Taylor Fitzgerald

Abstract The mechanism for initiating drizzle drop remains a gap in the current understanding of warm rain formation. One prevalent hypothesis suggests that the presence of Giant Cloud Condensation Nuclei (GCCN) generates drizzle-sized drops necessary to trigger the Collision-Coalescence (C-C) process. In this study, this hypothesis is investigated using a novel framework that integrates in situ observations, remote sensing measurements, and idealized models. Results show that GCCN can efficiently generate drizzle drops through condensation, producing a broad Droplet Size Distribution (DSD) comparable to in situ observations. The large drizzle drop and broad DSD strongly facilitate C-C, further accelerating drizzle initiation. To compare with observation, the model-generated DSDs are used to generate radar Doppler spectra where radar reflectivity and Doppler skewness is estimated. The simulated radar quantities correspond well with radar observations, providing critical evidence for the GCCN-induced drizzle initiation mechanism.

Plain Language Summary The formation of rain drops in warm clouds is not well-understood in the cloud physics community due to a lack of understanding in the formation of their precursor: drizzle drop with diameters around 40 μm. To close this knowledge gap, one hypothesis is that the large aerosol particles (diameter >1 μm) can accelerate drizzle formation. In this study, this hypothesis is tested by designing a novel investigation framework that integrates theoretical models and observations from in situ and remote sensing-based instruments. Using this framework, the presence of large aerosol particles was shown to significantly accelerate drizzle drop formation in warm clouds through enhanced condensation and the C-C process. This study provides novel insights on integrating multiple tools for cloud microphysics research.

1. Introduction

Drizzle initiation is a critical but unsolved process in warm precipitation formation (VanZanten et al., 2005; Wood, 2012). To initiate rain, a cloud needs a broad Drop Size Distribution (DSD) with "drizzle drops" to efficiently trigger the collision-coalescence (C-C) process. Prior to drizzle initiation, cloud drops are activated at cloud base where growth is controlled by condensation, which is inversely proportional to drop size. For this reason, condensational growth alone typically leads to narrow cloud DSD widths. The size difference between the cloud and drizzle drop (normally between 20 μm ~ 40 μm) cannot be well explained by C-C nor condensation (Yau & Rogers, 1996). A lack of understanding of this critical step makes it challenging to represent warm-rain processes in models and causes large prediction uncertainty (Lebsock et al., 2013; Morrison et al., 2020; Pathak et al., 2020).

Several mechanisms have been proposed to explain the drizzle drop formation (Feingold et al., 1999; Pinsky & Khain, 1997; Shaw, 2003). One hypothesis is based on the presence of Giant Cloud Condensation Nuclei (GCCN) with diameters >1 μm (Jensen & Nugent, 2017; Johnson, 1982; Mordy, 1959; Woodcock, 1950). As drops containing GCCN remain concentrated salt solutions, the saturated water vapor pressure over their surface is reduced, mitigating the supersaturation requirement for condensational growth. For instance, Jensen and Nugent (2017) proposed that drops formed on GCCN can grow through condensation in cloudy downdrafts and can grow to drizzle drops more readily. Once the drizzle drops are formed, the C-C process is efficiently triggered and further accelerates drizzle formation (Johnson, 1982).

Most studies of GCCN's effect on drizzle initiation use large eddy simulations (LES) and parcel models (Feingold et al., 1999; Jensen & Lee, 2008). Direct observational evidence is lacking due to the challenge of identifying the drizzle initiation process. In situ measurements provide accurate drizzle size information but are limited to specific field campaigns. On the other hand, remote sensing instruments provide long-term measurements, which are valuable for precipitation studies (Kollias, Clothiaux, et al., 2007). To detect drizzle drops in clouds, a common approach is identifying the region where radar reflectivity exceeds a threshold. The typical reflectivity threshold for drizzle detection varies from −20 dBZ to −15 dBZ (Frisch et al., 1995; Liu et al., 2008). However, Zhu et al. (2022) have demonstrated that radar reflectivity can be as low as −30 dBz when drizzle drops are present. To identify drizzle initiation, the skewness of radar Doppler spectrum is a more sensitive quantity and shows promise in detecting drizzle initiation (Acquistapace et al., 2019; Kollias, Rémillard, et al., 2011). Specifically, radar Doppler spectrum is the returned radar backscattering power distributed among radar Doppler velocity. In the absence of drizzle drop, the radar Doppler spectrum is systemic with skewness of zero. As drizzle drops form, the backscattering power in the "fast-falling regime" of the Doppler spectrum is enhanced, resulting in a skewed Doppler spectrum. Capitalizing on the Doppler spectrum shape allows the skewness to identify early formation of the drizzle drop. The Doppler spectrum skewness is a remote-sensing-based tool that, when used in combination with the modeling framework, provides insightful perspective on the drizzle initiation process. For instance, Kollias, Szyrmer, et al. (2011) applied a steady-state microphysical model coupled with radar forward model to simulate the initiation and growth of drizzle drop. The simulated radar signature during the drizzle formation process is consistent with radar observations.

In this study, we construct a novel framework to investigate the effect of GCCN on drizzle initiation in Stratocumulus (Sc). Specifically, idealized models are applied to bridge in situ aerosol properties observed at the surface, aircraft-based DSD measurements, and ground-based cloud radar observations. Using this framework, we demonstrate that the presence of GCCN in Sc accelerates drizzle initiation through both condensation and the Collision-Coalescence (C-C) mechanism.

2. Data and Methodology

This study's framework comprises a combination of in situ, remote sensing observation of aerosol-cloud properties, idealized cloud microphysical models, and radar forward simulator. Specifically, two cloud models are applied: a parcel model is used to simulate the activation of aerosol particles and condensation of cloud drop; a box model is used to simulate drop growth via the C-C process. To bridge the simulated cloud properties and radar measurements, a radar forward simulator is utilized to calculate radar quantities. Each component of methods and the data sets used in this study are described below.

2.1. Observational Data Sets

The observational data sets are adapted from the Aerosol and Cloud Experiments in the Eastern North Atlantic (ACE-ENA) field campaign operated by the Atmospheric Radiation Measurement (ARM) User Facility (Wang et al., 2022). The ACE-ENA campaign was conducted over the Graciosa Island from June 2017 to February 2018 during which the primary cloud system over the Graciosa Island is Sc which contains ubiquitous drizzle drop (Yang, Luke, et al., 2018; Zhu et al., 2022). During the campaign, a wide range of in situ and remote sensing instruments were operated to provide comprehensive measurements on aerosol and cloud properties. Here we will utilize the data sets observed during the Intensive Operational Period 2 (IOP2) from 11 January 2018 to 18 February 2018.

The Aerosol Observing System (AOS) is the primary platform for in situ aerosol measurements (Uin et al., 2019). Various instruments in the AOS measure the aerosol composition, size distribution, and hygroscopicity. The instruments utilized in this study are the Scanning Mobility Particle Sizer (SMPS) and the Aerodynamic Particle Sizer (APS). The SMPS measures the dry aerosol particle with diameter from 10 nm to 500 nm. The APS measures the particle aerodynamic diameters between 0.5 μm and 20 μm with large uncertainty near the tails of size range. The temporal resolution of SMPS and APS is 4 min and 1 min respectively. The original measurements are averaged over 1 hour to obtain the hourly mean aerosol concentration. Bins with zero aerosol concentration (i.e., empty bins) are included in the averaging to ensure that the hourly mean accounts for the bins with no detected particles. The averaged measurement is used to construct the aerosol size distribution with diameter from 20 nm to 10 μm, with size range from 20 nm to 0.5 μm from SMPS and size >1 μm from APS. The

distribution with size between 0.5 μm and 1 μm is linearly interpolated from the two instrument measurements. The GCCN is defined as the aerosol particle with diameter larger than 1 μm. For the APS and SMPS measurements, careful quality control procedures are performed by examining the sample pressure, impactor flow, flow relative humidity and instrument voltage (Shilling & Levin, 2023). As the aerosol sampled at high relative humidity could contain "wet" aerosols resulting from ambient water uptake, a dryer is applied for both instruments to maintain a dry environment. In practice, for SMPS the sampling air with RH higher than 20% is flagged as bad data and is excluded from the research (Singh & Kuang, 2024). For the APS, the sampling air with RH higher than 30% is excluded from this study. Thus the measured aerosol size from the APS and SMPS is considered as dry diameter.

The Surface Meteorology Systems (MET) provide temperature, relative humidity, and pressure near the surface with temporal resolution of 1 min. Observations from the AOS and MET are used as the input for the parcel model. The Ceilometer emits light at a wavelength of 910 nm and receives backscattered light from clouds, enabling the determination of cloud base height. The temporal resolution for the ceilometer is 30 s. The Ka ARM Zenith Radar (KAZR) is a vertical pointing radar operating with 35 GHz frequency and provides Doppler spectrum moments with 2 s temporal resolution and 30 m range resolution (Kollias, Miller, et al., 2007). To make the KAZR and ceilometer temporally matched, the ceilometer measurement is interpolated to the KAZR temporal space. Four radar Doppler spectrum moments: reflectivity, mean Doppler velocity (MDV), spectrum width and Doppler skewness are used in this study. The MDV is further used to retrieve the Eddy Dissipation Rate (EDR) using the algorithm detailed in Borque et al. (2016).The temporal resolution of the retrieved EDR product is 10 min. Finally, the Gulfstream 159 (G-1) research aircraft was operated to provide the in situ measured in-cloud liquid particle size distribution (DSD). Three cloud probes are adapted to measure the cloud/precipitation particle size distribution: the fast cloud droplet probe (FCDP) which measures the particle size distribution from 2 to 50 μm, the 2-dimensional stereo probe (2D-S) which measures the particle size distribution from 10 to 3,000 μm, and the high-volume precipitation spectrometer version 3 (HVPS-3) measuring the particle size distribution from 150 to 19,600 μm. A combined DSD product with particle diameter from 2 to 1, 000 μm is constructed from three probes by ARM. A comprehensive overview regarding the merged DSD product refers to Mei et al. (2024).

2.2. Modeling Framework

2.2.1. Parcel Model

The parcel model used in this study has been widely used to simulate warm cloud processes in previous studies (Feingold et al., 1998; Xue & Feingold, 2004; Yang, Kollias, et al., 2018; Yang et al., 2016). The parcel model simulates an adiabatically rising cloud parcel in which the aerosol particles are activated into cloud drops followed by condensational growth. The parcel model takes two inputs: the dry aerosol size distribution and the environmental thermodynamic. In this study, the input dry aerosol is adapted from the APS and SMPS measurements (Figure 4). A total of 140 bins is applied in the parcel model with diameter from 20 nm to 10 μm. A full list of the input dry aerosol size distribution can be downloaded from Zhu (2025). The input aerosol with diameter larger than 1 μm (i.e., GCCN) is assumed to be composed of sea salt, whereas the aerosol with diameter smaller than 1 μm is assumed to be composed of ammonium sulfate.

At the beginning of the simulation, the equilibrium haze particles are calculated using the dry aerosol particles assuming the supersaturation (S_{sat}) equals the environmental RH observed from MET. The S_{sat} of each aerosol particle is calculated through the Kohler equation:

$$S_{\text{sat}} = \frac{e}{e_s(T)} = a_s(r_d, r)\exp\left(\frac{2\sigma_s}{\rho_w R_v T r}\right)$$

where e is the water vapor pressure in air, e_s is the saturated water vapor pressure over the drop, ρ_w is the density of water and R_v is the gas constant of water vapor. σ_s is the surface tension, which is a function of temperature and solute mass (Pruppacher & Klett, 2012, p. 133). a_s is the water activity of haze droplets, which depends on the composition of aerosol, size of dry aerosol (r_d) and size of haze droplets (r). The a_s for sea salt and ammonium sulfate is calculated from the laboratory-based parameterizations (Cohen et al., 1987; Tang & Munkelwitz, 1994; Tang et al., 1997).

Once the equilibrium haze particles are calculated, the parcel is lifted upward, during which drops on a one-dimensional grid grow based on the local environment. A complete description of the governing equations of the parcel model is described in the Appendix.

2.2.2. Box Model

A box model is applied to simulate the growth of cloud drops through the C-C process. Specifically, a bin microphysical scheme based on Chen and Lamb (1994) is used in the box model to solve the Smoluchowski coagulation equation and predict the time evolution of droplet size distribution. The same scheme has been implemented in a large-eddy simulation model to explore drizzle initiation in a cloud chamber (Thomas et al., 2019; Wang et al., 2024; Yang et al., 2022). The collision kernel in the box model is adapted from Long (1974). Previous research has demonstrated that turbulence can enhance the collision efficiency and accelerate rain formation (Chandrakar et al., 2024; Sardina et al., 2015). To this end, we include the enhancement factor to the collision kernel based on the DNS simulated results in Chen et al. (2018, Table A1). It is noted that the collision enhancement is dependent on the flow dissipation rate. For instance, collision efficiency for drop with radius from 20 μm to 25 μm is increased by 10% with dissipation rate of 0.1 $m^2\ s^{-3}$ (Wang et al., 2005). For the clouds analyzed in this study, 85% of in-cloud EDR is lower than $10^{-3}\ m^2\ s^{-3}$ (shown in Figure 1c). Thus, turbulence is expected to play a minor role in the C-C process in this study.

2.2.3. Radar Doppler Spectrum Simulator

A novel aspect of this study is applying the radar Doppler spectrum simulator to convert the model outputs to radar-observed quantities, enabling direct comparison with KAZR observation. The radar spectrum simulator utilizes the DSD generated from the box model and generates the corresponding Doppler spectrum. The radar simulator parameters are adapted from KAZR configurations as detailed in Kollias et al. (2016). Particularly, the radar wavelength is set to 8.6 mm, the Nyquist velocity set as 5.96 $m\ s^{-1}$, Fast Fourier Transforms (FFT) length is set as 256. The turbulence broadening factor is set as 0.2 $m\ s^{-1}$, as indicated from KAZR observation. Radar reflectivity and spectrum skewness are estimated from the simulated Doppler spectrum to interpret the drizzle formation process. A detailed description of the radar simulator and its application in cloud microphysics studies refers to (Kollias, Rémillard, et al., 2011; Zhu et al., 2022).

3. Results

3.1. Case Overview

A typical Sc observed on 07 February 2018, is selected for investigation. Figure 1a shows 5 hr of radar observations for a cloud with thickness of around 300 m. Within the cloud layer, radar reflectivity increases from −25 dBZ to −15 dBZ from the cloud base to top; this pattern is explained by the condensational growth of cloud droplets. Even though the maximum radar reflectivity in this cloud is lower than −15 dBZ, virga with a depth up to 300 m is observed below the cloud base, indicating the presence of drizzle drops in the cloud as further validated from the in situ measurements. The MDV (Figure 1b) shows fluctuations from $-1.5\ m\ s^{-1}$ to $1.2\ m\ s^{-1}$. It is noted that strong updrafts mostly present within the cloud, while near-zero or negative velocity below cloud base. The prevalent downward motion in the sub-cloud layer is likely caused by drop evaporation. Figure 1c shows the retrieved EDR varies between $1.6*10^{-4}\ m^2\ s^{-3}$ and $5.8*10^{-3}\ m^2\ s^{-3}$ with the mean value of $5.7*10^{-4}\ m^2\ s^{-3}$, indicating a typical dynamical environment in Sc.

The temperature and humidity profiles from the sounding (Figure 2a) indicate that the boundary layer is well-mixed up to cloud top (∼1.5 km). From 17:35 UTC to 19:10 UTC, the G-1 aircraft flew through clouds with flight heights shown as the black line in Figure 1. Assuming the cloud properties are homogeneously distributed, the in situ measured DSDs over the observational sampling period (e.g., 17:35∼19:10 UTC) are averaged at each 50 m interval to represent the mean DSD in clouds (Figure 2b). It is shown that throughout the cloud layer, broad DSDs are identified with maximum drop diameter reaching to 500 μm. The drizzle drops, referring to drops with diameters larger than 40 μm, are present throughout the cloud. Close to the cloud top, the peak diameter of the DSD increases from 8 to 20 μm (blue to red line in Figure 2b) as a manifestation of condensational growth.

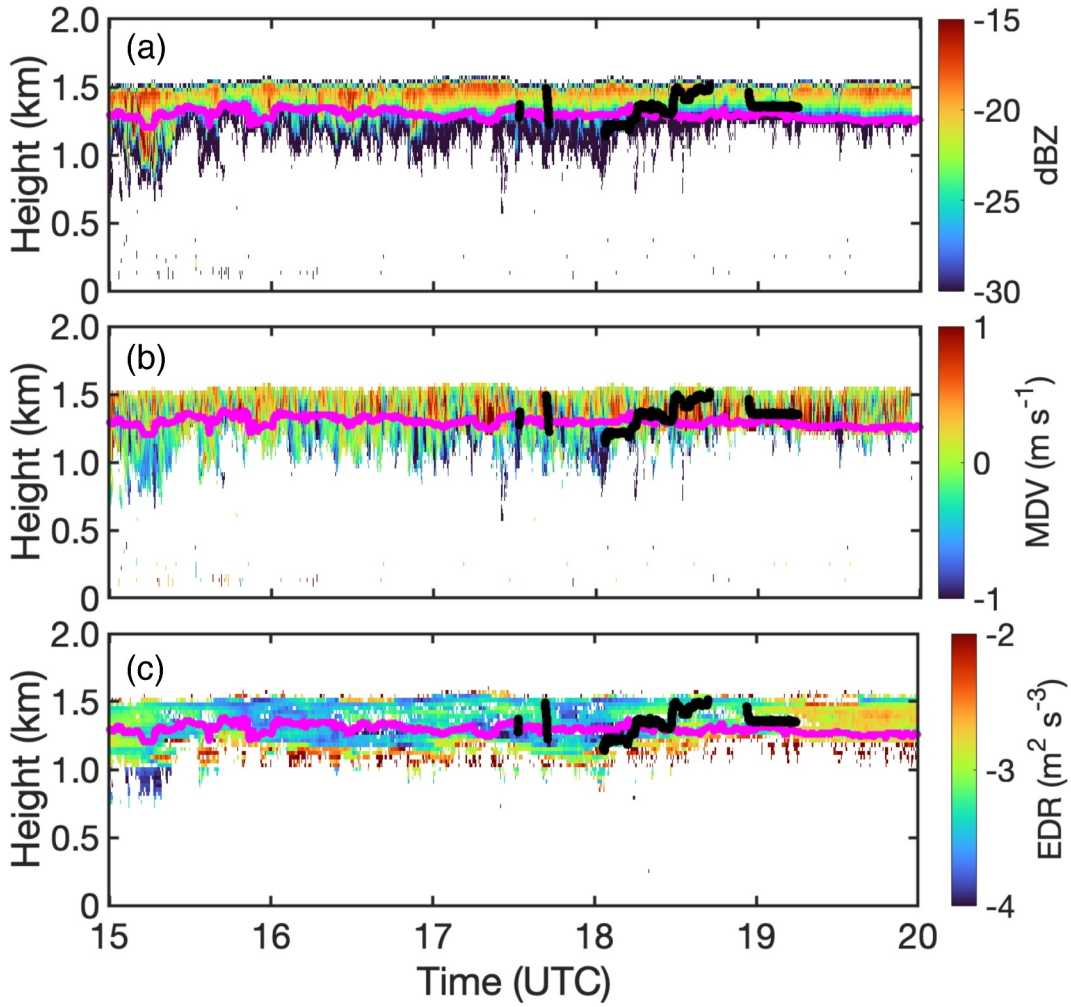

Figure 1. (a) Radar reflectivity (b) MDV and (c) EDR observed at ENA site on 7 February 2018 from 15 to 20 UTC. The magenta line represents cloud base height from ceilometer observation, the black line indicates the period and height where aircraft measurements are conducted.

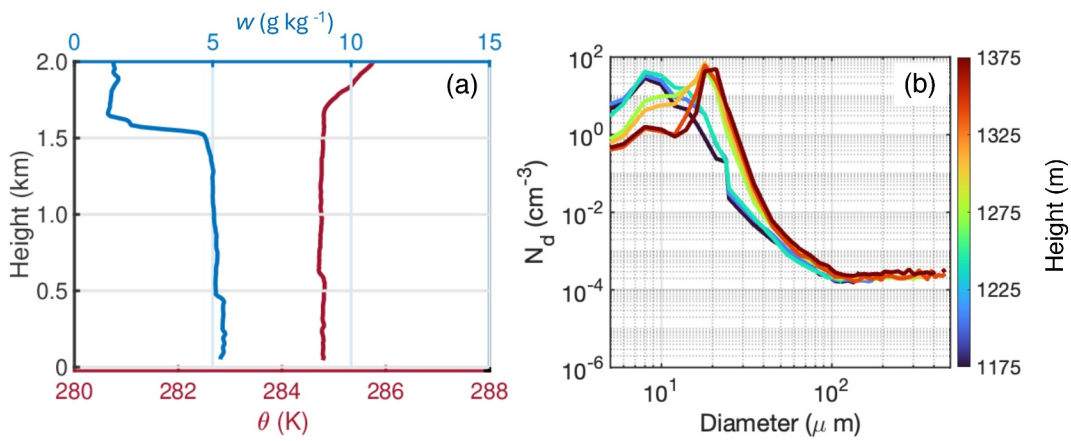

Figure 2. (a) Temperature and water vapor mixing ratio profiles from sounding at 17:42 UTC. (b) Averaged in-cloud DSD at various heights observed from the in situ measurements.

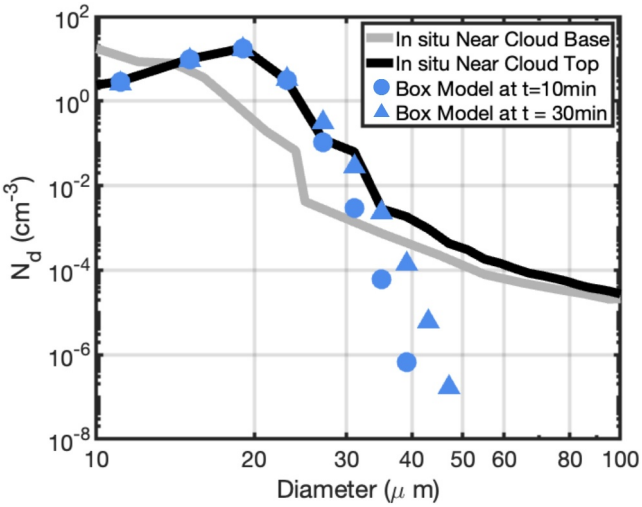

Figure 3. DSD from in situ measurements and box model simulation. The black line represents the in situ measured DSD near cloud top. The gray line represents in situ measured DSD near the cloud base. The circle symbol represents the box model-simulated DSD at 10 min, the triangle symbol represents the box model-simulated DSD at 30 min.

3.2. The Formation of Drizzle Drops Through C-C

The main question behind Figure 2b is how the drizzle drops are generated. First, we evaluate the effect of C-C on drizzle formation. In previous research, Chiu et al. (2021) applies the box model to simulate the C-C process in warm clouds with 10 min of residence time. In this study we exaggerate the C-C effect by conducting box model simulation for 30 min. To construct the input DSD of the box model, we collect the in situ measured DSDs near cloud top with height from 1,350 m to 1,400 m, from which the mean DSD is shown in Figure 3. We then truncate the DSD by removing drops with diameter larger than 30 μm. The reasoning of this step is that cloud drops rarely grow beyond 30 μm diameter without C-C process (Yau & Rogers, 1996). The truncated DSD is used as a box model input as the initial stage. The simulated DSDs at 10 and 30 min from the box model are shown in Figure 3.

It is shown that drops with diameter larger than 40 μm are generated, but with number concentration (N_d) significantly lower than in situ measurements (black line in Figure 3). At 10 min, the N_d of drop with 40 μm diameter is 10^{-6} cm^{-3}, which is almost 3 magnitudes lower than the in situ observation. The difference between the model simulation and in situ measurements is more prominent as drops grow larger. At 30 min of the simulation, the N_d of drop with 40 μm is one magnitude smaller than the in situ measurements, whereas the N_d of drop with 50 μm is 3 magnitudes smaller than measurements. Therefore, Figure 3 indicates that only through the C-C process, drizzle drops are not efficiently produced to be comparable with observation. Another interesting phenomenon in Figure 3 is the N_d of drizzle drop is higher at cloud top than near cloud base. This phenomenon is contrasting to the conventional thinking that drizzle drop are formed through C-C as they fall toward the cloud base. Instead, this behavior implies that drizzle drops grow as they ascend, which is likely due to the condensation growth of drops formed on GCCN.

3.3. The Formation of Drizzle Drop Through GCCN

In this section, we isolate the C-C process and only consider the effect of GCCN on drizzle formation. Since the boundary layer is well-mixed (Figure 2a), we assume that aerosols upon which cloud droplets are formed were transported from the surface. This is a reasonable assumption particularly for the GCCN which is generated by sea spray (Lewis & Schwartz, 2004; Quinn et al., 2015). The aerosol DSD was constructed with diameters from 20 nm to 10 μm using the AOS measurements collected from 18 to 19 UTC (Figure 4). In this study, the GCCN refers to the dry aerosol particle with diameter larger than 1 μm (blue line in Figure 4). Using the constructed aerosol DSD as the input, the parcel model was applied with predefined updraft velocity of 0.5 ms^{-1} to simulate drop activation and condensation processes. The fidelity of the applied updraft velocity is validated by the KAZR mean Doppler velocity (Figure 1b).

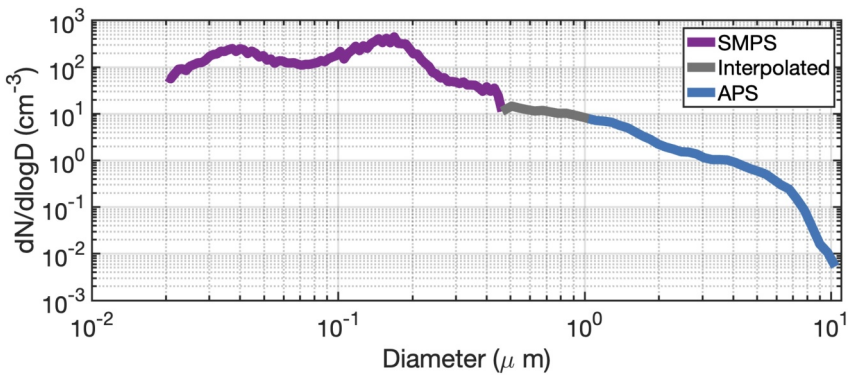

Figure 4. The averaged aerosol size distribution from 17 to 18 UTC on 7 February 2018 constructed from AOS: aerosol with dry diameter smaller than 0.5 μm is obtained from SMPS (purple line), aerosol with dry diameter larger than 1 μm is obtained from APS shown as blue line. Aerosol distribution in between is linearly interpolated shown as the gray line.

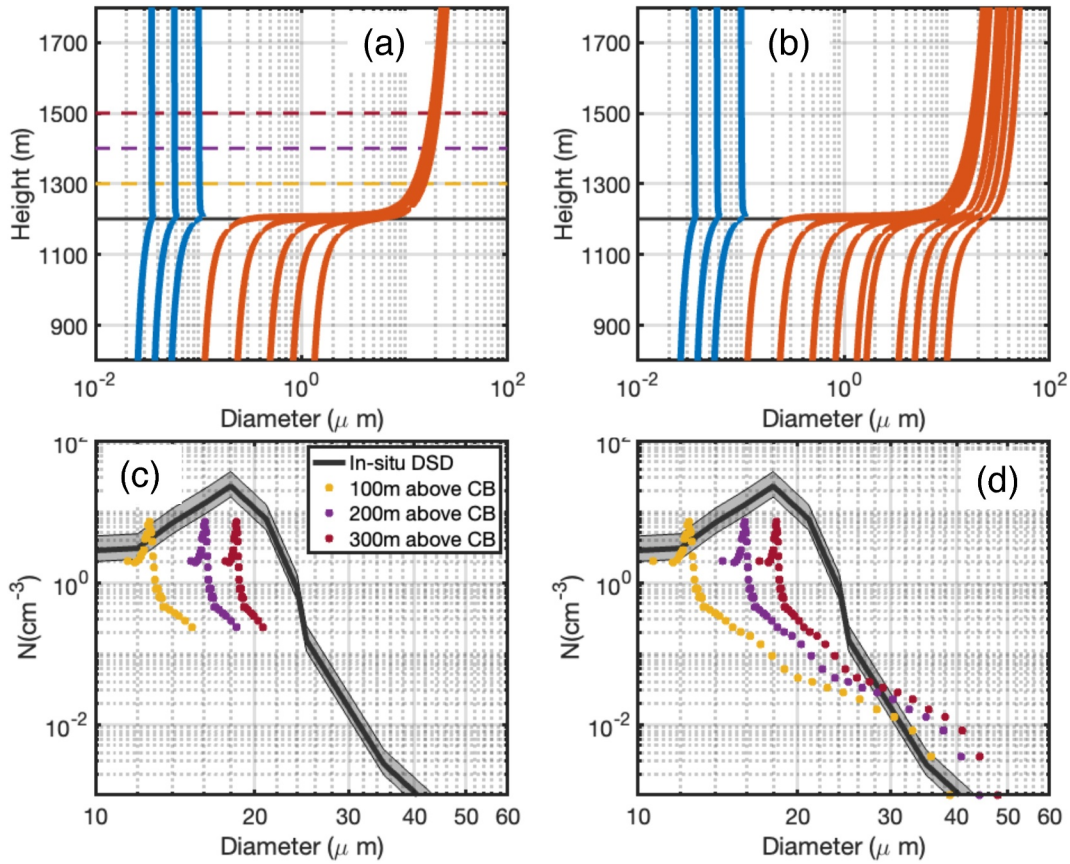

Figure 5. Parcel model output showing particle grows with height for the simulations (a) excluding and (b) including GCCN. Blue lines indicate the inactivated aerosol particles and orange lines represent the activated cloud droplets. The horizontal solid black line represents the cloud base height. The horizontal dash lines shown in (a) represent the height of 100 m (yellow), 200 m (purple), and 300 m (red) above cloud base. (c) The DSD at 100 m (yellow dots), 200 m (purple dots), and 300 m (red dots) above cloud base from the parcel model simulation excluding GCCN. The black line indicates the in situ observed DSD at 300 m above cloud base. Panels (d): same as (c) but including GCCN. The gray shading over the in situ measured DSD in (c) and (d) represent the 25 and 75 percentiles of the measured N_d.

Using the constructed dry aerosol size distribution, two sensitivity experiments are conducted with different inputs: (a) the full aerosol DSD including GCCN and (b) the aerosol DSD with diameter <1 μm, excluding GCCN. The dry aerosol particles are used to calculate the equilibrium haze particles by assuming the super-saturation (S_{sat}) equals the environment RH observed from the MET observation during 18–19 UTC, which is 59%. The equilibrium haze drops then grow through condensation simulated by the parcel model.

In both experiments, drops grow as a function of height (Figures 5a and 5b). Aerosol particles with diameters larger than 0.1 μm are activated to cloud drops (orange lines) whereas the others (blue lines) remain as haze drops. Unlike the experiment without GCCN (Figure 5a), the experiment with GCCN (Figure 5b) produces large drops that continue to grow within the cloud and can reach drizzle-size drops. For instance, for the dry aerosol with diameters of 10 μm, the corresponding drop diameter at 300 m above cloud base is 53 μm, which is comparable to the previous parcel model simulations (Jensen & Nugent, 2017). This result reinforces that GCCN can serve as cloud condensation nuclei and directly form drizzle drops through condensational growth.

To illustrate the differences between the simulated cloud DSD with/without GCCN, distributions at three heights above the cloud base are selected (Figures 5c and 5d). It is noted that, for both simulations, DSDs shift to the large size regime as height increases, indicating condensation contributing to particle growth. However, noticeable differences can be characterized for the experiment with/without GCCN: the simulated DSD without GCCN has a narrow distribution with maximum drop diameter of 21 μm; in contrast, the simulation with GCCN has a much broader DSD with a longer tail where 50 μm diameter droplet being generated.

Impressively, the simulated DSD for the GCCN experiment is comparable to the in situ observations (black line in Figure 5d). First, the peak DSD diameter at 300 m above cloud base (red dots) is ∼18 μm, closely aligning with peak DSD diameter in the in situ measurements. Second, the number concentration of the particles with diameter ∼30 μm is approximately the same magnitude between the simulation and observation. However, a difference is also noticed where the in situ measured DSD is much broader than the simulated DSD, especially for the drop diameter <25 μm. Several mechanisms are accounting for this inconsistency. First, the absence of entrainment mixing process in the parcel model. Previous studies have indicated that mixing processes can broaden the DSD and trigger drizzle formation through the C-C process (Pinsky & Khain, 2018; Tölle & Krueger, 2014). A lack of entrainment mixing in the parcel model may produce a narrow DSD. Second, artifacts involved in in situ measurements can lead to the broader observed DSD. Particularly, a recent study (Allwayin et al., 2024) utilizes high-resolution in situ measurements showing the cloud DSD is more narrow at small scales than at whole-cloud averages. For this case, the in situ measurements are averaged over 2 hr with thousands of sampled DSDs, thus the broad DSD shown in Figure 5 may be caused by the averaging artifacts.

Another noticeable difference in Figure 5d is the N_d of drops with diameters >30 μm is greater in the simulated DSD compared to in situ measurements. This is potentially caused by the assumption that all the measured GCCN at the surface are transported into the cloud layer. In reality, only a fraction of the GCCN is transported upward into the cloud due to their large inertia and fast sedimentation velocity (Lewis & Schwartz, 2004). Reducing the input GCCN concentration in the parcel model leads to more comparable results for drop diameter larger than 30 μm (not shown). It is noted, however, that the purpose of this study is not conducting simulation to match the in situ measurements. The novelty of this study is to propose a framework integrating in situ, remote sensing measurements and idealized models to provide an insight of the GCCN effect on drizzle formation. Overall, the large N_d discrepancy in the drizzle regime in Figure 3 and results in Figure 5d indicate that, for the presented case, GCCN plays a critical role on the drizzle formation through condensational growth alone.

3.4. The Formation of Drizzle Drop With Combined GCCN and C-C Effect

Once drizzle drops (i.e., diameter >40 μm) are formed, the C-C mechanism becomes efficient and can further accelerate drizzle production. Thus, it is expected that in the presence of GCCN, drizzle drops would be produced more efficiently along with the C-C process. To test this hypothesis, two box-model simulations are conducted (one with and one without GCCN) with the initial DSDs from the parcel-model-generated DSDs (red dots in Figures 5c and 5d). The box model simulations are conducted for 1 hr with timestep of 2 s. To quantify the drizzle production during the C-C process, we define two parameters: drizzle mass ratio (R_d) and drizzle production rate (P_d). The R_d represents the mass ratio between the drizzle regime and total liquid water within the parcel. P_d represents the increment of drizzle mass per second in a one cubic meter parcel.

$$R_d = \frac{m_d}{m_t}$$

$$P_d = \frac{\Delta m_d}{\Delta t}$$

Where m_d represents the total mass for the drizzle drop (i.e., diameter larger than 40 μm) and m_t represents the total liquid mass in the parcel. Δm_d represents the change of drizzle mass in each time step Δt (i.e., 2 s). The P_d unit is g s^{-1} m^{-3} whereas R_d is dimensionless.

Figure 6 shows that the C-C process produces drizzles more efficiently in the presence of GCCN. For the experiment without GCCN, drizzle start to form as soon as the C-C process is triggered (blue line in Figure 6a). However, the production rate is very slow at the beginning and takes a long time to produce sufficient drizzle mass. Specifically, 10 min after the C-C process is triggered, the drizzle production rate is only 1.5*10^{-10} g s^{-1} m^{-3} (Figure 6b), and the drizzle mass ratio of 2.5*10^{-8} (Figure 6a). On the contrary, at the same time (i.e., 10 mins after the C-C process), the drizzle production rate for the experiment with GCCN is 2.6*10^{-6} g s^{-1} m^{-3}, the drizzle mass ratio is 4*10^{-3}. As the simulation continues, drizzle production rate increases for both scenarios. But P_d and R_d for the GCCN experiment is always higher than the experiment without GCCN. At the end of the 1-hr simulation, R_d for the GCCN experiment is 18 times higher than the experiment without GCCN. The R_d and P_d without GCCN are approximately the same value of the initial GCCN experiment input. In other words, including GCCN in the presented case accelerates drizzle production almost 1 hour ahead.

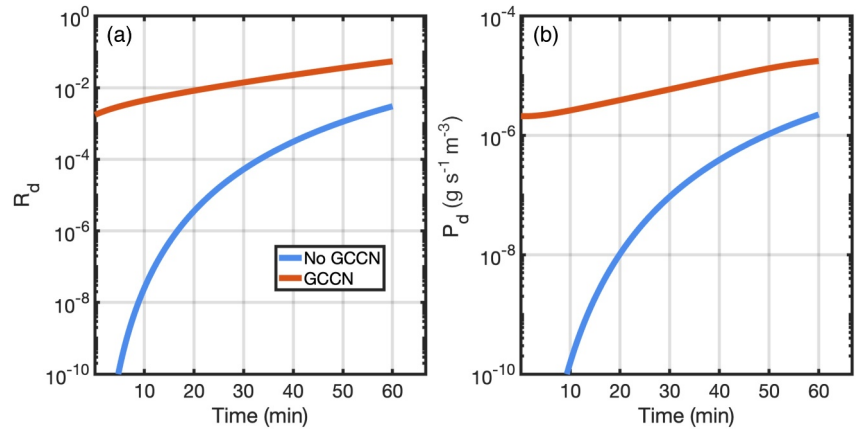

Figure 6. (a) Drizzle mass ratio and (b) drizzle production rate simulated from a box model for two experiments: the blue line represents the No GCCN experiment, and the orange line represents the GCCN experiment.

3.5. Effect of GCCN on Drizzle Initiation From Cloud Radar Perspective

In previous sections, we applied two idealized models to separately consider the effect of GCCN and C-C processes on drizzle production. We concluded that, for the presented case in the study, without GCCN, C-C alone is unlikely to produce sufficient number of drizzle drops which is comparable to observation. In this section we conduct a statistical analysis to testify the effect of GCCN on drizzle initiation using cloud radar observations. Using the vertical pointing radar measurements (i.e., KAZR used in this study), the observed radar Doppler spectrum can characterize the DSD evolution and interpret the microphysical process. A skewed radar Doppler spectrum is manifested as the unbalanced backscattering power received from drizzle and cloud drops. If the downward velocity is defined as the positive direction, then the presence of drizzle embryos generates a positive Doppler skewness value (Luke & Kollias, 2013). Previous studies have demonstrated that Doppler skewness is a sensitive indicator for drizzle existence and can detect drizzle embryos with reflectivity as low as −30 dBZ (Zhu et al., 2022).

To test the effect of GCCN on drizzle initiation, three experiments were performed using varying GCCN input with 1%, 20%, and 50% of the GCCN spectrum shown in Figure 4. As the total GCCN number concentration is 2.5 cm^{-3}, the corresponding GCCN concentration for these three groups is 0.025, 0.5, and 1.25 cm^{-3} respectively. We follow the similar procedures in Section 3.2 and Section 3.3, the newly constructed aerosol spectrum is input for the parcel model to generate DSD at 300 m above cloud base, which is then used as the input for a 1-hr box model simulation. For the box model-generated DSDs, the radar simulator is applied to emulate the Doppler spectrum and to estimate radar reflectivity and Doppler skewness. One example of such simulation is shown in Figure 7, the box model-generated DSD indicates the presence of drizzle drop with diameter larger than 40 μm, corresponds to the Doppler spectrum with skewness of 0.12 and radar reflectivity of −21 dBZ. For each experiment, 1,800 pairs of spectrum-reflectivity values are generated with 1-hr simulation. The mean Doppler skewness is calculated for the reflectivity range between −26 dBZ and −22 dBZ with 2 dB interval. To compare the Doppler skewness for different GCCN-sensitivity experiments, the mean Doppler skewness is normalized by their maximum value in each simulation group. The relationship between radar reflectivity and normalized skewness for the three sensitivity experiments is shown in Figure 8a.

Figure 8a shows that for the three experiments, skewness increases as the reflectivity increases from −26 dBZ to −22 dBZ. This feature is consistent with previous studies (Kollias, Rémillard, et al., 2011; Luke et al., 2008) and indicates the formation of drizzle drops. However, a clear difference on the skewness value is identified for different GCCN experiments: for the higher GCCN concentration scenario, larger skewness is characterized for the same reflectivity value. Larger skewness represents the radar backscattering power from drizzle particles is higher than the one from cloud droplets, indicating that more drizzle particles were generated as GCCN concentrations increase. The skewness difference is more significant with reflectivity smaller than −23 dBZ, indicating the GCCN effect is more efficient in the early stage of drizzle initiation.

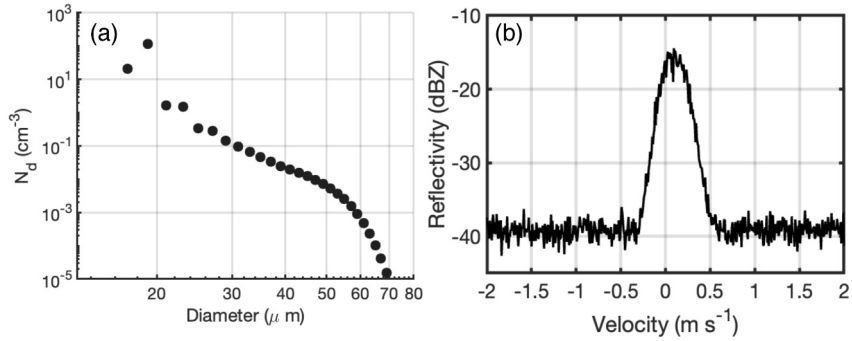

Figure 7. An example showing the simulated DSD (a) from the box model at 15 min for the GCCN included experiment. (b) Simulated radar Doppler spectrum corresponding to (a), from which the radar reflectivity and Doppler skewness is calculated as −21 dBZ, 0.12, respectively.

This skewness-reflectivity relationship is further validated from KAZR observation. Here, 38 days of the KAZR observations during the IOP-2 period are utilized along with the APS-measured GCCN at surface. The GCCN concentration is calculated as the hourly-averaged concentration of aerosol particles with diameters >1 μm. The distribution of the total GCCN concentration is shown in Figure 9a, with the peak of 1.5 cm^{-3} and the largest value around 12 cm^{-3}. Based on the distribution, three GCCN groups are selected with GCCN number concentration (N_{GCCN}) < 2 cm^{-3}, 2 cm^{-3} < N_{GCCN} < 4 cm^{-3} and 4 cm^{-3} < N_{GCCN}. In each group, the hourly-mean radar Doppler skewness as a function of reflectivity is calculated. Similarly to the skewness normalization process for the model output, the observed Doppler skewness is normalized by the maximum value in each N_{GCCN} group. Previous studies have suggested the effect of turbulence on drizzle formation in cumulus clouds. In cumulus, typical EDR value is on the order of 10^{-2} m^2 s^{-3}, strong turbulence enhances the collision efficiency between drops to produce drizzle efficiently. In Sc, the EDR is relatively small. For the radar data used in this study, 85% of the in-cloud EDR is smaller than 10^{-3} m^2 s^{-3} (Figure 9b). To eliminate the potential effect of large turbulence on the drizzle formation, we only use the radar data with EDR value smaller than 10^{-3} m^2 s^{-3}. Under such a small turbulence environment, the effect of the turbulence on the C-C process is limited. Finally, to reduce the likelihood that the particles detected by the APS are remnants of evaporated precipitation, only KAZR observations with virga depths smaller than 300 m are considered. The virga depth is defined as the vertical extent of significant radar echoes below the cloud base height. The relationship between the observed reflectivity and skewness is shown in Figure 8b.

Radar measurements (Figure 8b) echo the simulation results (Figure 8a) showing large skewness for high N_{GCCN}. The skewness for N_{GCCN} > 4 cm^{-3} is larger than the skewness for N_{GCCN} < 2 cm^{-3} with a significant value of 5% for reflectivity smaller than −24 dBZ. Similar to the modeling result, the skewness difference is more prominent for small reflectivity values where the skewness value is lower. This phenomenon indicates the role of GCCN on

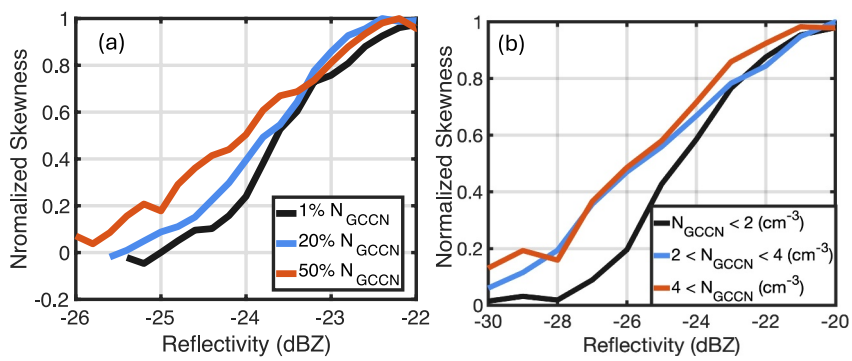

Figure 8. (a): Normalized skewness (details are shown in the text) as a function of radar reflectivity with different GCCN concentration simulations: black line for 1% of GCCN, blue line for 20% of GCCN, orange line for 50% of GCCN. Panels (b): Same as (a) but from KAZR observation. Black, blue, and orange line represents different concentrations of GCCN as shown in the legend. The bin boundaries at 2 and 4 cm^{-3} are not included in the group classification.

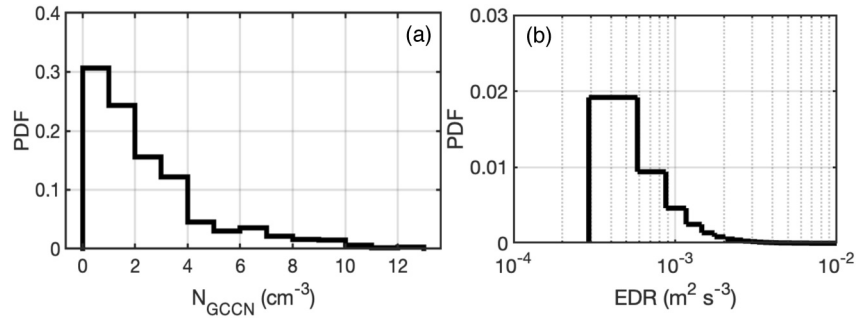

Figure 9. Distribution of the (a) hourly averaged GCCN concentration and the (b) retrieved EDR during the ACE-ENA IOP2 field campaign.

drizzle production through C-C is more prominent at the drizzle initiation stage. The skewness does not exhibit a significant difference for the group of $N_{GCCN} > 2$ cm^{-3} and the group of 2 cm^{-3} < N_{GCCN} < 4 cm^{-3}. Nevertheless, Figure 8 shows consistent behavior between modeling and observation that Doppler radar spectrum is larger under higher N_{GCCN} environment, demonstrating large GCCN concentration favors drizzle formation.

4. Conclusion

In this study we conducted a novel framework by combining idealized models, in situ measurements, and remote sensing observation to investigate the impact of GCCN in drizzle formation. We first analyze a Sc case with cloud thickness around 300 m with drizzle drops being produced throughout the clouds. To understand the formation of these drizzle drops, we examine two mechanisms: the C-C process and GCCN. While investigating the C-C mechanism, the in situ measured DSD near the cloud top is truncated to only include cloud drops. The truncated DSD is fed into the box model for 30-min simulation. The simulated DSDs show much lower concentration of drizzle drops compared to the in situ measurements, indicating the C-C alone is not efficient enough to produce the amount of drizzle suggested by observation.

Next, we test the effect of GCCN on drizzle formation though the condensation process. The in situ measured aerosol size distribution from the AOS and the thermodynamical property observed at the surface are used to initialize the parcel model to simulate cloud droplet activation and condensational growth. Two simulations are conducted with/without GCCN included. The simulation including GCCN shows a broad DSD with a long tail, whose morphology is comparable to the aircraft-based in situ measurements; whereas the simulation without GCCN has a narrow DSD and fails to generate drizzle droplets. This experiment suggests that including GCCN in the model is sufficient to produce drizzle drops comparable to in situ measurements.

We then combine these two mechanisms to investigate the C-C process on drizzle initiation in the presence of GCCN. The DSD output from the parcel model is fed into a box model to simulate the collisional growth of drops. 1 hour of simulation is conducted for both experiments (with and without GCCN). The box model results indicate that the presence of GCCN enhances the drizzle production rate and generates more drizzle mass compared to the experiment without GCCN. Finally, radar observations are compared to validate the effect of GCCN on drizzle initiation. A radar simulator was used to emulate the Doppler spectrum corresponding to the DSD output from the box model. Radar reflectivity and skewness were estimated from the Doppler spectrum for different GCCN concentration experiments. For a given radar reflectivity, higher GCCN concentration corresponded to larger skewness, consistent with the KAZR observations, which demonstrated that GCCN facilitated drizzle initiation.

Our results indicate that GCCN can facilitate drizzle formation through two mechanisms: (a) cloud/haze drops formed on GCCN can grow to drizzle-size drops (~40 μm) through condensational growth more readily. (b) The large drops formed on GCCN broaden the DSD and can further accelerate drizzle growth through the C-C process. Among other potential factors influencing drizzle formation, one aspect we did not emphasize is the effect of turbulence. Studies have indicated that small-scale turbulence enhances the C-C efficiency among cloud drops and favors drizzle formation (Chandrakar et al., 2024; Pinsky & Khain, 1997; Shaw, 2003; Zhu et al., 2023). In this study, since the research target is Sc, turbulence is small and is not expected to play a significant role in the C-C enhancement. However, the turbulence generating process, for example, entrainment mixing, may impact the

drizzle formation by broadening the cloud DSD (Krueger et al., 1997; Tölle & Krueger, 2014). To distinguish the various effects and quantify their contribution to the drizzle initiation puzzle, well-controlled experiments conducted in the laboratory facility (e.g., cloud chamber) are required in future study.

Appendix A: Governing Equations for the Parcel Model

The prognostic variables of the parcel model are air pressure (p), height (h), air temperature (T), water vapor mixing ratio (q_v) and radius of droplets (r)

The air pressure (p) is calculated from the hydrostatic equation:

$$dp = -\rho_a g dh \tag{A1}$$

Where ρ_a is the air density, g is the gravitational acceleration.

Height (h) is calculated from the initial height (h_0) and the assigned air velocity (w):

$$h = h_0 + \mathrm{wt} \tag{A2}$$

Air temperature (T) is calculated from:

$$\frac{dT}{dt} = -\frac{g}{c_p} w + \frac{l_v}{c_p} \frac{dq_w}{dt} \tag{A3}$$

Where c_p is the heat capacity of air, l_v is the latent heat of water vapourization and q_w is the liquid water mixing ratio. As the total water mixing ratio is conserved in the parcel, a decrease/increase in water vapor mixing ratio (dq_v) equals the increase/decrease in liquid water mixing ratio (dq_w).

$$dq_v = -dq_w \tag{A4}$$

The growth of droplet (r) is calculated from:

$$\frac{dr}{dt} = \frac{1}{r} \frac{S_e - S_{\mathrm{sat}}}{G} \tag{A5}$$

Where G is the growth parameter given by:

$$G = \left[\frac{\rho_w R_v T}{D_v e_s(T)} + \frac{\rho_w l_v}{k_T T} \left(\frac{l_v}{R_v T} - 1 \right) \right] \tag{A6}$$

Where R_v is the gas constant for water vapor and ρ_w is the density of water. D_v and k_T are the physical diffusion coefficient of water vapor and the thermal diffusion coefficient. D_v and k_T are calculated from (Lamb & Verlinde, 2011, pp. 337–338).

The governing equations from Equations A1 to A6 are solved using a variable-coefficient ordinary differential equation solver (VODE) developed by (Brown et al., 1989).

Conflict of Interest

The authors declare no conflicts of interest relevant to this study.

Data Availability Statement

The KAZR data (kazrge) is accessed via Atmospheric Radiation Measurement (ARM) user facility. 2015. Ka ARM Zenith Radar (KAZRGE), 2018-01-11 to 2018-02-18, Eastern North Atlantic (ENA) Graciosa Island, Azores, Portugal (C1). Compiled by N. Bharadwaj, I. Lindenmaier, K. Johnson, D. Nelson, B. Isom, J. Hardin, A.

Matthews, T. Wendler, V. Melo de Castro, M. Deng, M. Rocque and Y. Feng. ARM Data Center. [Dataset]. at http://dx.doi.org/10.5439/1984772.

The ceilometer dataset (ceil) can be accessed via Zhang, D., Ermold, B., & Morris, V. Ceilometer (CEIL), 2018-01-11 to 2018-02-18, Eastern North Atlantic (ENA), Graciosa Island, Azores, Portugal (C1). Atmospheric Radiation Measurement (ARM) User Facility. [Dataset]. https://doi.org/10.5439/1181954.

The sounding data set can be accessed via: Keeler, E., Coulter, R., & Kyrouac, J. Balloon-Borne Sounding System (SONDE), 2018-01-11 to 2018-02-18, Eastern North Atlantic (ENA), Graciosa Island, Azores, Portugal (C1). Atmospheric Radiation Measurement (ARM) User Facility. [Dataset]. https://doi.org/10.5439/1971077.

The Surface Meteorological Instrumentation (MET) observation can be accessed via: Kyrouac, J., Shi, Y., & Tuftedal, M. Surface Meteorological Instrumentation (MET), 2018-01-11 to 2018-02-18, Eastern North Atlantic (ENA), Graciosa Island, Azores, Portugal (C1). Atmospheric Radiation Measurement (ARM) User Facility. [Dataset]. https://doi.org/10.5439/1786358.

The Doppler spectrum simulator is accessed via Zhu (2023). Physics-based Doppler Spectrum Simulator (V0.1.0) [Software]. Zenodo. https://doi.org/10.5281/zenodo.7897981.

Acknowledgments
Z. Zhu, F. Yang and M. Zawadowicz were funded by the Department of Energy (DOE) as part of the Atmospheric System Research (ASR) program under Contract DE-SC0012704. A. Rincon, J. Ritvanen, S. Lankowicz, K. H. Lundstrom, T. Fitzgerald were supported by the NSF the Facilities for Atmospheric Research and Education (FARE) Program (Award 2113070).

References

Acquistapace, C., Löhnert, U., Maahn, M., & Kollias, P. (2019). A new criterion to improve operational drizzle detection with ground-based remote sensing. *Journal of Atmospheric and Oceanic Technology*, *36*(5), 781–801. https://doi.org/10.1175/jtech-d-18-0158.1

Allwayin, N., Larsen, M. L., Glienke, S., & Shaw, R. A. (2024). Locally narrow droplet size distributions are ubiquitous in stratocumulus clouds. *Science*, *384*(6695), 528–532. https://doi.org/10.1126/science.adi5550

Borque, P., Luke, E., & Kollias, P. (2016). On the unified estimation of turbulence eddy dissipation rate using Doppler cloud radars and lidars. *Journal of Geophysical Research: Atmospheres*, *121*(10), 5972–5989. https://doi.org/10.1002/2015jd024543

Brown, P. N., Byrne, G. D., & Hindmarsh, A. C. (1989). VODE: A variable-coefficient ODE solver. *SIAM Journal on Scientific and Statistical Computing*, *10*(5), 1038–1051. https://doi.org/10.1137/0910062

Chandrakar, K. K., Morrison, H., Grabowski, W. W., & Lawson, R. P. (2024). Are turbulence effects on droplet collision–coalescence a key to understanding observed rain formation in clouds? *Proceedings of the National Academy of Sciences of the United States of America*, *121*(27), e2319664121. https://doi.org/10.1073/pnas.2319664121

Chen, J.-P., & Lamb, D. (1994). Simulation of cloud microphysical and chemical processes using a multicomponent framework. Part I: Description of the microphysical model. *Journal of the Atmospheric Sciences*, *51*(18), 2613–2630. https://doi.org/10.1175/1520-0469(1994)051<2613:socmac>2.0.co;2

Chen, S., Yau, M., & Bartello, P. (2018). Turbulence effects of collision efficiency and broadening of droplet size distribution in cumulus clouds. *Journal of the Atmospheric Sciences*, *75*(1), 203–217. https://doi.org/10.1175/jas-d-17-0123.1

Chiu, J. C., Yang, C. K., Van Leeuwen, P. J., Feingold, G., Wood, R., Blanchard, Y., & Wang, J. (2021). Observational constraints on warm cloud microphysical processes using machine learning and optimization techniques. *Geophysical Research Letters*, *48*(2), e2020GL091236. https://doi.org/10.1029/2020gl091236

Cohen, M. D., Flagan, R. C., & Seinfeld, J. H. (1987). Studies of concentrated electrolyte solutions using the electrodynamic balance. 2. Water activities for mixed-electrolyte solutions. *Journal of Physical Chemistry*, *91*(17), 4575–4582. https://doi.org/10.1021/j100301a030

Feingold, G., Cotton, W. R., Kreidenweis, S. M., & Davis, J. T. (1999). The impact of giant cloud condensation nuclei on drizzle formation in stratocumulus: Implications for cloud radiative properties. *Journal of the Atmospheric Sciences*, *56*(24), 4100–4117. https://doi.org/10.1175/1520-0469(1999)056<4100:tiogcc>2.0.co;2

Feingold, G., Walko, R., Stevens, B., & Cotton, W. (1998). Simulations of marine stratocumulus using a new microphysical parameterization scheme. *Atmospheric Research*, *47*, 505–528. https://doi.org/10.1016/s0169-8095(98)00058-1

Frisch, A., Fairall, C., & Snider, J. (1995). Measurement of stratus cloud and drizzle parameters in ASTEX with a K_{α}-band Doppler radar and a microwave radiometer. *Journal of the Atmospheric Sciences*, *52*(16), 2788–2799. https://doi.org/10.1175/1520-0469(1995)052<2788:moscad>2.0.co;2

Jensen, J. B., & Lee, S. (2008). Giant sea-salt aerosols and warm rain formation in marine stratocumulus. *Journal of the Atmospheric Sciences*, *65*(12), 3678–3694. https://doi.org/10.1175/2008jas2617.1

Jensen, J. B., & Nugent, A. D. (2017). Condensational growth of drops formed on giant sea-salt aerosol particles. *Journal of the Atmospheric Sciences*, *74*(3), 679–697. https://doi.org/10.1175/jas-d-15-0370.1

Johnson, D. B. (1982). The role of giant and ultragiant aerosol particles in warm rain initiation. *Journal of the Atmospheric Sciences*, *39*(2), 448–460. https://doi.org/10.1175/1520-0469(1982)039<0448:trogau>2.0.co;2

Kollias, P., Clothiaux, E. E., Ackerman, T. P., Albrecht, B. A., Widener, K. B., Moran, K. P., et al. (2016). Development and applications of ARM millimeter-wavelength cloud radars. *Meteorological Monographs*, *57*, 17.11–17.19. https://doi.org/10.1175/amsmonographs-d-15-0037.1

Kollias, P., Clothiaux, E. E., Miller, M. A., Albrecht, B. A., Stephens, G. L., & Ackerman, T. P. (2007). Millimeter-wavelength radars: New frontier in atmospheric cloud and precipitation research. *Bulletin of the American Meteorological Society*, *88*(10), 1608–1624. https://doi.org/10.1175/bams-88-10-1608

Kollias, P., Miller, M. A., Luke, E. P., Johnson, K. L., Clothiaux, E. E., Moran, K. P., & Albrecht, B. A. (2007). The Atmospheric Radiation Measurement Program cloud profiling radars: Second-generation sampling strategies, processing, and cloud data products. *Journal of Atmospheric and Oceanic Technology*, *24*(7), 1199–1214. https://doi.org/10.1175/jtech2033.1

Kollias, P., Rémillard, J., Luke, E., & Szyrmer, W. (2011). Cloud radar Doppler spectra in drizzling stratiform clouds: 1. Forward modeling and remote sensing applications. *Journal of Geophysical Research*, *116*(D13), D13201. https://doi.org/10.1029/2010jd015237

Kollias, P., Szyrmer, W., Rémillard, J., & Luke, E. (2011). Cloud radar Doppler spectra in drizzling stratiform clouds: 2. Observations and microphysical modeling of drizzle evolution. *Journal of Geophysical Research*, *116*(D13), D13203. https://doi.org/10.1029/2010jd015238

Krueger, S. K., Su, C.-W., & McMurtry, P. A. (1997). Modeling entrainment and finescale mixing in cumulus clouds. *Journal of the Atmospheric Sciences*, *54*(23), 2697–2712. https://doi.org/10.1175/1520-0469(1997)054<2697:meafmi>2.0.co;2

Lamb, D., & Verlinde, J. (2011). *Physics and chemistry of clouds*. Cambridge University Press.

Lebsock, M., Morrison, H., & Gettelman, A. (2013). Microphysical implications of cloud-precipitation covariance derived from satellite remote sensing. *Journal of Geophysical Research: Atmospheres*, *118*(12), 6521–6533. https://doi.org/10.1002/jgrd.50347

Lewis, E. R., & Schwartz, S. E. (2004). *Sea salt aerosol production: Mechanisms, methods, measurements, and models* (Vol. 152). American Geophysical Union.

Liu, Y., Geerts, B., Miller, M., Daum, P., & McGraw, R. (2008). Threshold radar reflectivity for drizzling clouds. *Geophysical Research Letters*, *35*(3), L03807. https://doi.org/10.1029/2007gl031201

Long, A. B. (1974). Solutions to the droplet collection equation for polynomial kernels. *Journal of the Atmospheric Sciences*, *31*(4), 1040–1052. https://doi.org/10.1175/1520-0469(1974)031<1040:sttdce>2.0.co;2

Luke, E. P., & Kollias, P. (2013). Separating cloud and drizzle radar moments during precipitation onset using Doppler spectra. *Journal of Atmospheric and Oceanic Technology*, *30*(8), 1656–1671. https://doi.org/10.1175/jtech-d-11-00195.1

Luke, E. P., Kollias, P., Johnson, K. L., & Clothiaux, E. E. (2008). A technique for the automatic detection of insect clutter in cloud radar returns. *Journal of Atmospheric and Oceanic Technology*, *25*(9), 1498–1513. https://doi.org/10.1175/2007jtecha953.1

Mei, F., Comstock, J. M., Pekour, M. S., Fast, J. D., Gaustad, K. L., Schmid, B., et al. (2024). Atmospheric Radiation Measurement (ARM) airborne field campaign data products between 2013 and 2018. *Earth System Science Data*, *16*(11), 5429–5448. https://doi.org/10.5194/essd-16-5429-2024

Mordy, W. (1959). Computations of the growth by condensation of a population of cloud droplets. *Tellus*, *11*(1), 16–44. https://doi.org/10.3402/tellusa.v11i1.9283

Morrison, H., van Lier-Walqui, M., Fridlind, A. M., Grabowski, W. W., Harrington, J. Y., Hoose, C., et al. (2020). Confronting the challenge of modeling cloud and precipitation microphysics. *Journal of Advances in Modeling Earth Systems*, *12*(8), e2019MS001689. https://doi.org/10.1029/2019ms001689

Pathak, R., Sahany, S., & Mishra, S. K. (2020). Uncertainty quantification based cloud parameterization sensitivity analysis in the NCAR community atmosphere model. *Scientific Reports*, *10*(1), 17499. https://doi.org/10.1038/s41598-020-74441-x

Pinsky, M., & Khain, A. (2018). Theoretical analysis of the entrainment–mixing process at cloud boundaries. Part I: Droplet size distributions and humidity within the interface zone. *Journal of the Atmospheric Sciences*, *75*(6), 2049–2064. https://doi.org/10.1175/jas-d-17-0308.1

Pinsky, M. B., & Khain, A. P. (1997). Turbulence effects on droplet growth and size distribution in clouds—A review. *Journal of Aerosol Science*, *28*(7), 1177–1214. https://doi.org/10.1016/s0021-8502(97)00005-0

Pruppacher, H. R., & Klett, J. D. (2012). *Microphysics of clouds and precipitation: Reprinted 1980*. Springer Science & Business Media.

Quinn, P. K., Collins, D. B., Grassian, V. H., Prather, K. A., & Bates, T. S. (2015). Chemistry and related properties of freshly emitted sea spray aerosol. *Chemical Reviews*, *115*(10), 4383–4399. https://doi.org/10.1021/cr500713g

Sardina, G., Picano, F., Brandt, L., & Caballero, R. (2015). Continuous growth of droplet size variance due to condensation in turbulent clouds. *Physical Review Letters*, *115*(18), 184501. https://doi.org/10.1103/physrevlett.115.184501

Shaw, R. A. (2003). Particle-turbulence interactions in atmospheric clouds. *Annual Review of Fluid Mechanics*, *35*(1), 183–227. https://doi.org/10.1146/annurev.fluid.35.101101.161125

Shilling, J. E., & Levin, M. S. (2023). *Scanning mobility particle sizer (smps)-aerodynamic particle sizer (Aps) merged size distribution (mergedsmpsaps) value-added product report*. Oak Ridge National Laboratory.

Singh, A., & Kuang, C. (2024). *Scanning mobility particle sizer (SMPS) instrument handbook*. ARM Climate Research Facility.

Tang, I., & Munkelwitz, H. (1994). Water activities, densities, and refractive indices of aqueous sulfates and sodium nitrate droplets of atmospheric importance. *Journal of Geophysical Research*, *99*(D9), 18801–18808. https://doi.org/10.1029/94jd01345

Tang, I. N., Tridico, A., & Fung, K. (1997). Thermodynamic and optical properties of sea salt aerosols. *Journal of Geophysical Research*, *102*(D19), 23269–23275. https://doi.org/10.1029/97jd01806

Thomas, S., Ovchinnikov, M., Yang, F., van der Voort, D., Cantrell, W., Krueger, S. K., & Shaw, R. A. (2019). Scaling of an atmospheric model to simulate turbulence and cloud microphysics in the Pi chamber. *Journal of Advances in Modeling Earth Systems*, *11*(7), 1981–1994. https://doi.org/10.1029/2019ms001670

Tölle, M. H., & Krueger, S. K. (2014). Effects of entrainment and mixing on droplet size distributions in warm cumulus clouds. *Journal of Advances in Modeling Earth Systems*, *6*(2), 281–299. https://doi.org/10.1002/2012ms000209

Uin, J., Aiken, A. C., Dubey, M. K., Kuang, C., Pekour, M., Salwen, C., et al. (2019). Atmospheric Radiation Measurement (ARM) aerosol observing systems (AOS) for surface-based in situ atmospheric aerosol and trace gas measurements. *Journal of Atmospheric and Oceanic Technology*, *36*(12), 2429–2447. https://doi.org/10.1175/jtech-d-19-0077.1

VanZanten, M., Stevens, B., Vali, G., & Lenschow, D. (2005). Observations of drizzle in nocturnal marine stratocumulus. *Journal of the Atmospheric Sciences*, *62*(1), 88–106. https://doi.org/10.1175/jas-3355.1

Wang, A., Ovchinnikov, M., Yang, F., Schmalfuss, S., & Shaw, R. A. (2024). Designing a convection-cloud chamber for collision-coalescence using large-eddy simulation with bin microphysics. *Journal of Advances in Modeling Earth Systems*, *16*(1), e2023MS003734. https://doi.org/10.1029/2023ms003734

Wang, J., Wood, R., Jensen, M. P., Chiu, J. C., Liu, Y., Lamer, K., et al. (2022). Aerosol and cloud experiments in the eastern North Atlantic (ACE-ENA). *Bulletin of the American Meteorological Society*, *103*(2), E619–E641. https://doi.org/10.1175/bams-d-19-0220.1

Wang, L.-P., Ayala, O., Kasprzak, S. E., & Grabowski, W. W. (2005). Theoretical formulation of collision rate and collision efficiency of hydrodynamically interacting cloud droplets in turbulent atmosphere. *Journal of the Atmospheric Sciences*, *62*(7), 2433–2450. https://doi.org/10.1175/jas3492.1

Wood, R. (2012). Stratocumulus clouds. *Monthly Weather Review*, *140*(8), 2373–2423. https://doi.org/10.1175/mwr-d-11-00121.1

Woodcock, A. H. (1950). Condensation nuclei and precipitation. *Journal of the Atmospheric Sciences*, *7*(2), 161–162. https://doi.org/10.1175/1520-0469(1950)007<0161:cnap>2.0.co;2

Xue, H., & Feingold, G. (2004). A modeling study of the effect of nitric acid on cloud properties. *Journal of Geophysical Research*, *109*(D18), D18204. https://doi.org/10.1029/2004jd004750

Yang, F., Kollias, P., Shaw, R. A., & Vogelmann, A. M. (2018). Cloud droplet size distribution broadening during diffusional growth: Ripening amplified by deactivation and reactivation. *Atmospheric Chemistry and Physics*, *18*(10), 7313–7328. https://doi.org/10.5194/acp-18-7313-2018

Yang, F., Luke, E. P., Kollias, P., Kostinski, A. B., & Vogelmann, A. M. (2018). Scaling of drizzle virga depth with Cloud thickness for marine Stratocumulus clouds. *Geophysical Research Letters*, *45*(8), 3746–3753. https://doi.org/10.1029/2018gl077145

Yang, F., Ovchinnikov, M., Thomas, S., Khain, A., McGraw, R., Shaw, R. A., & Vogelmann, A. M. (2022). Large-eddy simulations of a convection cloud chamber: Sensitivity to bin microphysics and advection. *Journal of Advances in Modeling Earth Systems*, *14*(5), e2021MS002895. https://doi.org/10.1029/2021ms002895

Yang, F., Shaw, R., & Xue, H. (2016). Conditions for super-adiabatic droplet growth after entrainment mixing. *Atmospheric Chemistry and Physics*, *16*(14), 9421–9433. https://doi.org/10.5194/acp-16-9421-2016

Yau, M. K., & Rogers, R. R. (1996). *A short course in cloud physics*. Elsevier.

Zhu, Z. (2025). Aerosol size distribution for parcel model input [Dataset]. *Zenodo*. https://doi.org/10.5281/zenodo.17610980

Zhu, Z., Kollias, P., Luke, E., & Yang, F. (2022). New insights on the prevalence of drizzle in marine stratocumulus clouds based on a machine learning algorithm applied to radar Doppler spectra. *Atmospheric Chemistry and Physics*, *22*(11), 7405–7416. https://doi.org/10.5194/acp-22-7405-2022

Zhu, Z., Yang, F., Kollias, P., & Luke, E. (2023). Observational investigation of the effect of turbulence on microphysics and precipitation in warm marine boundary layer clouds. *Geophysical Research Letters*, *50*(10), e2022GL102578. https://doi.org/10.1029/2022gl102578